

${}^6\text{LiF}:\text{ZnS}(\text{Ag})$ Mixture Optimization for a Highly Efficient Ultrathin Cold Neutron Detector

A. Osovizky, K. Pritchard, J. Ziegler, E. Binkley, Y. Yehuda-Zada, P. Tsai, A. Thompson, C. Cooksey, K. Siebein, N. Hadad, M. Jackson, C. Hurlbut, R. Ibberson, G. M. Baltic, C. F. Majkrzak, and N. C. Maliszewskyj

Abstract—We report the optimization of ${}^6\text{LiF}:\text{ZnS}(\text{Ag})$ scintillator mixtures for an ultrathin (< 2 mm), highly efficient cold neutron detector. Preliminary results with early prototypes demonstrated excellent absorption for 3.62 meV (4.75 Å wavelength) neutrons but mediocre neutron sensitivity ($\approx 30\%$).

Our optimization took the form of exploring the weight ratios of neutron converter, phosphor, and binder to promote high neutron capture probability and light transport within the medium. We characterized a series of ${}^6\text{LiF}:\text{ZnS}(\text{Ag})$:Binder mixtures for neutron absorption, light yield, and light transmission properties. In the process we determined the optimal configuration for our requirements of millimeter thickness and cold neutron energy.

Optimized prototypes exhibit excellent absorption and demonstrate neutron sensitivities of above 85 % for 3.27 meV neutrons and gamma ray rejection ratios approaching 10^{-7} .

Index Terms— Neutron detector, $\text{LiF}:\text{ZnS}(\text{Ag})$, CANDOR, WLS fiber

I. INTRODUCTION

THE Chromatic Analysis Neutron Diffractometer Or Reflectometer [1] (CANDOR) spectrometer under development at the NIST Center for Neutron Research is a new concept for an instrument used to determine the structure of materials. Traditional diffractometers or reflectometers use several means to select out and direct a beam of neutrons of a specific incident energy onto a sample under test. Neutrons scattered from this sample are then detected by a neutron sensitive detector.

In the CANDOR instrument, a polychromatic (“white”) beam of neutrons is directed onto a sample and neutrons scattered from the sample will pass through arrays of highly oriented pyrolytic graphic (HOPG) crystals set at different angles with respect to the centerline of each array. Neutrons of the appropriate energy will be Bragg diffracted by the crystals

into an associated neutron detector. By collecting the scattered radiation into energy bins simultaneously it is possible to perform measurements as much as an order of magnitude more efficiently than is currently possible on a traditional instrument of this type.

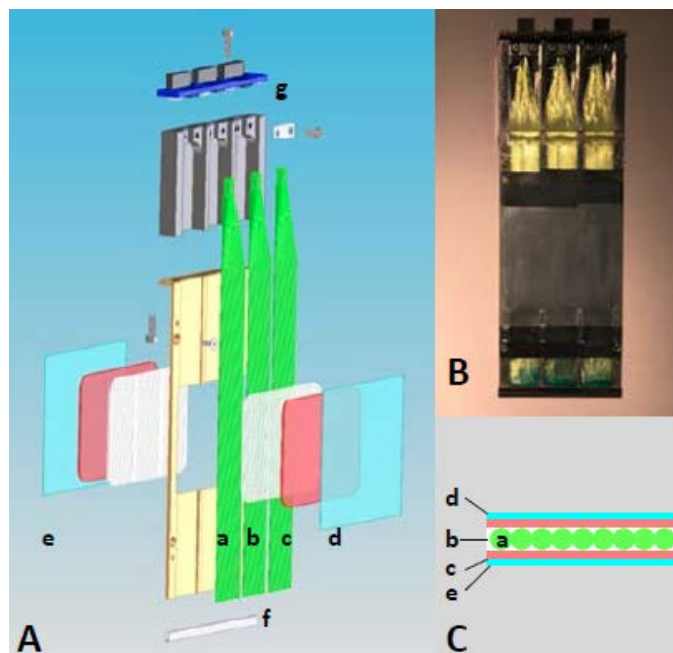


Figure 1: Anatomy of CANDOR scintillator detector. The detector module consists of three detection units arranged side by side. A: Exploded view of triple frame detector module. Wavelength shifting fibers (a) are laid side by side in an aluminum frame. Layer (b) consists of a Ni-doped 1:2:0.6 scintillator “primer”. Slabs of scintillator (c) backed with either Alanod reflector (d) or Vikuiti reflector (e) are pressed around the primed fiber. A terminal reflector (f) is wrapped around the WLS fiber end. The SiPMs are mounted on a carrier board (g) mating to the WLS fibers. B: Photograph of the assembled detector. C: Cross section of the assembled layers.

To achieve this speed of measurement (and to more efficiently use the neutrons produced by our reactor), it is

Submitted on October 10, 2017. This work was supported in part by the U.S. Department of Commerce.

A. Osovizky is with the University of Maryland, College Park, MD on leave from Rotem Industries and the Nuclear Research Center Negev (email: alon@rotemi.co.il).

K. Pritchard (email: kevin.pritchard@nist.gov), J. Ziegler (email: jeffrey.ziegler@nist.gov), E. Binkley (email: ed.binkley@nist.gov), P. Tsai (email: peter.tsai@nist.gov), A. Thompson (email: akt@nist.gov), C. Cooksey (email: catherine.cooksey@nist.gov), K. Siebein (email: kerry.siebein@nist.gov), N. Hadad (email: nancy.hadad@nist.gov), R.

Ibberson, G. M. Baltic (email: george.baltic@nist.gov), C. F. Majkrzak (email: charles.majkrzak@nist.gov), and N. C. Maliszewskyj (email: nickm@nist.gov) are with the National Institute of Standards and Technology, Gaithersburg, MD 20899 USA. R. Ibberson is now with Oak Ridge National Lab, Oak Ridge TN 37831 USA (email: ibbersonrm@ornl.gov).

Y. Yehuda-Zada is with the Nuclear Research Center Negev, Beer Sheva Israel. (email: kobyzada@gmail.com).

M. Jackson (email: mjackson@eljentechnology.com) and C. Hurlbut (email: churlbut@eljentechnology.com) are with Eljen Technology, Sweetwater TX 79556 USA.

essential to have as many of these energy-analyzing channels as possible packed into a tight angular range. If the neutron detector is exceedingly thin (≈ 2 mm), the reflectometer can accommodate several of these analyzing channels over an increased angular range of reflected neutrons.

The anatomy of the neutron detector is shown in Figure 1 [2]. Slabs of $6\text{LiF}:\text{ZnS}(\text{Ag})$ scintillator are formed around a close-packed array of wavelength shifting (WLS) fibers (0.5 mm diameter Kuraray Y-11) which conduct the scintillation light out of the plane of the detector to a photosensor.

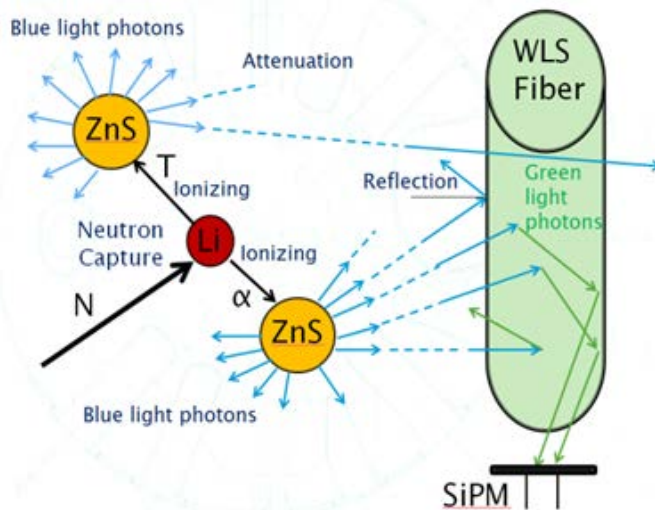


Figure 2: Neutron detection mechanism. Neutrons are captured by 6Li and liberate an alpha particle and a triton, which in turn ionize the ZnS phosphor. Blue light emitted by the phosphor travels through the scintillator to be captured in the wavelength shifting (WLS) fiber, which shifts the wavelength to green and transmits those photons to a photosensor.

The scintillator has a high 6Li atom density of $10^{22}/\text{cm}^3$ [3] resulting in about 95% capture efficiency for 3.62 MeV neutrons at 1 mm thickness as given by Equation 1 where σ is the cross section [cm^2], ρ is the atoms density [$1/\text{cm}^3$] and L is the detector depth [cm] [4].

$$\frac{I}{I_0} = e^{-\sigma\rho L} \quad (1)$$

The Li is provided in the form of the salt 6LiF to prevent decomposition. In a neutron capture reaction, an alpha particle and a triton are produced with high Q (definition) value: $6\text{Li} + n \rightarrow \text{Triton} (2.74 \text{ MeV}) + \text{Alpha} (2.06 \text{ MeV})$ [5] [6] [7]. These particles ionize the $\text{ZnS}(\text{Ag})$, resulting in the emission of light photons. About 55,000 photons [8] are produced by the ionization of $\text{ZnS}(\text{Ag})$ by a 1 MeV alpha particle. The light yield for the capture of a single neutron is estimated at 160,000 photons [9] [10].

The basic principle of neutron detection using this device requires two conversions as shown in Figure 2. A cold neutron enters the sensor and is captured by the 6Li in the scintillator. The alpha particle and triton are ejected in opposite directions. These reaction products travel for only a few microns in the scintillator medium, ionizing the $\text{ZnS}(\text{Ag})$ phosphor. The ionized $\text{ZnS}(\text{Ag})$ emits blue light photons with a luminescence wavelength of 450 nm [11]. Because the alpha and triton can lose energy before ionizing the phosphor and the neutron

capture location is a distance from the WLS fiber, the measured number of scintillation photons can vary among neutron capture events. Only a small portion of the emitted light photons travelling through the largely opaque scintillator will reach the WLS fiber [12].

Upon entering the WLS fiber, the blue scintillation photons are absorbed by the fluorescent dye in the wavelength shifting fiber. Green light photons (≈ 476 nm) are then emitted by the dye and are transported along the fiber to a silicon photomultiplier used as the photosensor. About 5% of the light emitted in the fiber optic bundle is transported to the photosensor [13].

The main characteristic distinguishing a neutron capture event from other types is the duration of the event. Thermal events (in the photosensor) are very short-lived, on the order of tens of nanoseconds. Gamma ray capture events are also short, on the order of 90 ns. Neutron capture events, however, are typically longer than 200 ns with photons arriving at the photosensor in irregular bursts. For this reason, pulse shape discrimination (PSD) techniques are the most effective for distinguishing neutron capture events from other types. The challenge in signal processing is to strike a balance between discriminating even the weakest neutron capture signal from other signal types while not inhibiting the ability to count at reasonable rates (> 10 kHz).

To experience the highest neutron possible neutron sensitivity, it is essential that neutron capture events with strong and weak signals are successfully discriminated. To ensure that photons from occurring at the very edge of the scintillator reach the WLS fibers and photosensor with a sufficient population to be discriminated it is crucial that we be able to improve light production and transport in the large opaque scintillator medium while preserving neutron absorption.

Our preliminary results measured with an early prototype detector yielded the desired neutron absorption ($\approx 95\%$ for 3.27 MeV neutrons). The measured neutron sensitivity, however, was poor (about 30%). To bring this performance closer to that of 3He in an ultrathin package, it is necessary to optimize the composition of the scintillator and the configuration of sensor to preserve neutron absorption while enhancing light transport and collection.

II. EXPERIMENTAL

The overall detector neutron sensitivity is dependent on both the neutron capture probability and the measurability of the light signal. Therefore, efforts to optimize the sensor should focus on the composition of the scintillator, the configuration of the wavelength shifting fibers, and additional enhancements such as reflectors.

For the sake of simplicity, we will refer to the scintillator composition using a three-part weight ratio $6\text{LiF}:\text{ZnS}(\text{Ag})$:binder corresponding to the principal components of the 6LiF neutron converter, the $\text{ZnS}(\text{Ag})$ phosphor, and the organic binder holding them together. Clearly, the number density of 6Li atoms for a given thickness of material is the chief parameter driving neutron capture probability. For the daughter products of the neutron capture reaction to ionize the phosphor, the $\text{ZnS}(\text{Ag})$ grains must be

near the ${}^6\text{LiF}$. However, the opacity of the $\text{ZnS}(\text{Ag})$ phosphor to its own luminescence presents a stumbling block to the goal of having both high neutron capture probability and intense light production and transmission. Fortunately, the inert binder material present in sufficient quantities can enhance light transport in the scintillator mixture so its concentration becomes an easily tunable parameter.

For the studies we performed we have used a formulation of the scintillator which used ethanol as the solvent, so as not to attack the polystyrene in the WLS fibers.

We have used the GEANT 4 (Geometry ANd Tracking) simulation package to model both the neutron capture reaction and light transport in the medium. Geant4 [14] is a platform for the simulation of particles passing through matter using Monte Carlo methods and includes libraries for handling geometry, tracking, detector response, run management, and visualization. It can realistically model the optics of scintillation including light photon production and light transport considering its attenuation and reflection.

Because the simple composition of the scintillator is not enough to determine the material properties, we used microscopy and light transmission measurements to determine the morphology and light transport characteristics.

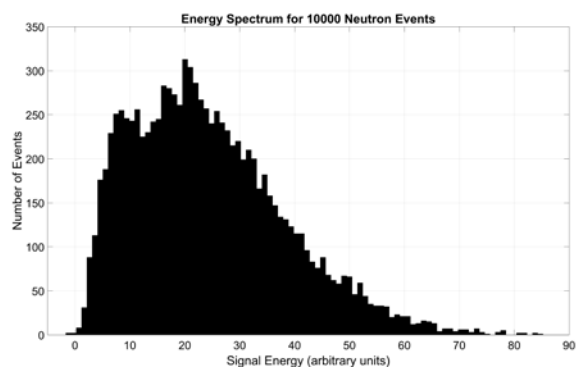


Figure 3: Pulse height distribution of neutron capture events

Samples of the scintillator mixture were imaged using a Carl Zeiss Ultra 60 Free Electron Scanning Electron Microscope [15] equipped with an Oxford Instruments X-Max 80 Silicon Drift Detector (SDD) for Energy Dispersive X-ray (EDS) Analysis. The samples were imaged using the Everhart Thornley (SE2) detector to reveal the particle morphology, and the Energy Selective Backscatter Detector (EsB) which provides a material atomic number contrast. Materials containing elements of higher atomic number appear brighter in the images. EDS analysis was used to determine the elemental composition of the particles and binder. The samples were imaged in the condition received from the manufacturer.

The samples were also used for wavelength dependent light transmission measurements to determine the mixture's light transport properties. The transmittance measurements were made using a Perkin Elmer Lambda1050 UV/Vis/NIR spectrophotometer. For regular transmittance measurements, the spectrophotometer's standard detector module was used. The dimensions of the incident beam were approximately 3 mm by 7 mm and centered on the front surface of the frame at an

angle of incidence of nominally 0° . For diffuse transmittance measurements, the standard detector module was replaced with an integrating sphere module and the dimensions of the incident beam were like the one used during the regular transmittance measurements. The sphere had a diameter of 150 mm, an oval entrance port of about 15 mm by 25 mm, a sample port diameter nominally of 25 mm, and a coating of sintered polytetrafluoroethylene (PTFE). The illuminating source was a quartz-tungsten-halogen (QTH) incandescent lamp, and the detector was a photomultiplier tube (PMT). The measurements were performed over the wavelength range from 400 nm to 500 nm by depolarizing the incident beam using a 30-mm depolarizing element. This wavelength region is comparable with the $\text{ZnS}(\text{Ag})$ light wavelength emission.

All measurements requiring neutrons were performed at the NG1 detector development station at the NIST Center for Neutron Research. On this instrument, the neutrons were monochromated to 3.62 meV (4.75 Å wavelength) with a beam flux of ≈ 4800 n/cm²/sec over an area of 0.28 cm². For neutron absorption measurements (neutron capture probability) we used a ${}^3\text{He}$ reference detector to compare the beam current with and without the scintillator sensor in place. In order to compare various ${}^6\text{LiF}:\text{ZnS}(\text{Ag})$:Binder ratios, samples supported on frames with glass plate backings were filled with the different mixtures. The thickness of the frame was 0.43mm.

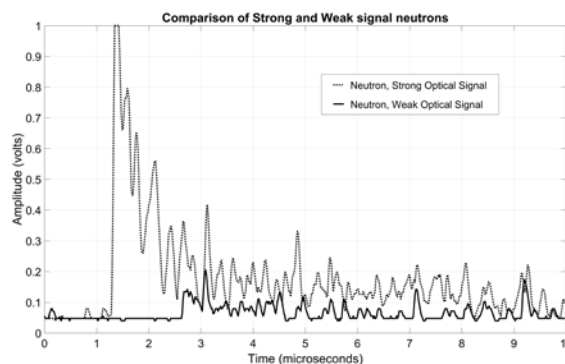


Figure 4: Comparison of strong and weak neutron capture signatures. Regardless of the strength of the initial peak they are very long lived (many microseconds).

We used the SensL C-series (FC30035) silicon photomultiplier (SiPM) as a photosensor operating at 2.5 V above the breakdown voltage. The signal from the SiPM was fed into a fast amplifier with a gain matched to the dynamic range of an ADC operating at 250 million samples per second. The digitized signal was processed by a Xilinx Virtex FPGA (definition) running a pulse shape discrimination algorithm. [16] The FPGA produced logic pulses as output with each successfully discriminated neutron event. For rapid comparisons between different detector configurations, we also used a multichannel analyzer to obtain pulse height distributions. Example waveforms for both strong and weak neutron capture events are shown in Figure 4.

III. OPTIMIZING THE SCINTILLATOR

The detector sensitivity is determined by both the neutron capture probability (a function of ${}^6\text{Li}$ density) and the detectable

light output produced by the ZnS(Ag) ionization which is transmitted through the medium and collected by the photosensor. The target figure for the absorption of 3.27 meV (5 Å) neutrons in our assembly is 95%. If the system can recognize 95 % of those capture events, the net detection sensitivity will be 90 %.

These two goals are in conflict in an ultrathin (< 2mm) detector. For maximal absorption, the scintillator mixture should contain a high concentration of ${}^6\text{Li}$. However, to get high light yield it should contain a high concentration of ZnS(Ag), preferably in a form that enhances the possibility of phosphor ionization by the neutron capture products. Furthermore, the opacity of ZnS(Ag) to its own luminescence also requires that the concentration of the transparent binder be increased to ensure that scintillator photons can exit the scintillator medium without being reabsorbed. A schematic description of the interplay of these interactions is shown in Figure 5.

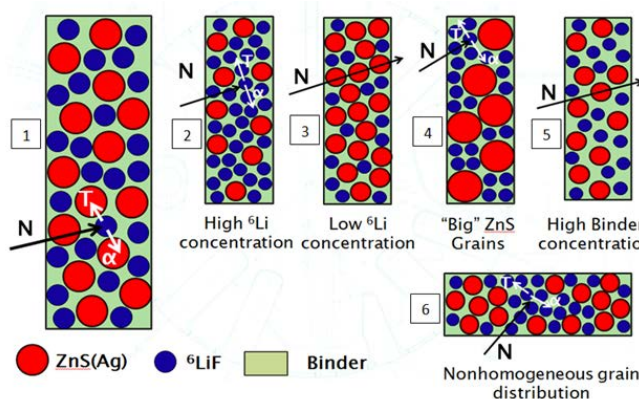


Figure 5: Schematic representations of scintillator components in the compound and optimal arrangements. (1) An optimal configuration in which neutron capture products ionize the phosphor producing light. (2) Too much Li makes for high probability of neutron capture but low light production. (3) Too little Li in the mixture will not stop incident neutrons. (4) If the ZnS grains are too large there is a possibility that one of the neutron capture reaction products will not deposit its energy in the phosphor. (5) Too much binder results in low neutron capture probability. (6) An inhomogeneous distribution of phosphor grains (clustering) will result in the same characteristics as large grains

Our preliminary finding, which showed high neutron capture with weak light signature, prompted us to focus on increasing the transparency of the medium by adding binder to the mixture. We varied the binder concentrations from 0.3 weight percent up to 0.75 keeping the proportion of ${}^6\text{LiF}$ and ZnS fixed in slabs of identical thickness (Table 1). The fact that increases in the light transmission level off at the weight ratio of 1:2:0.6 demonstrate that there is a limit to the improvement in light transmission that can be achieved by simply increasing the proportion of binder.

We also tried to improve the light transmission by adding glass beads to the mixture. The glass beads improved the light transmission (2.58 %) compared to a measurement of the same mixture (1:2:0.3) without the glass beads (1.85 %), but at the cost of dramatically reducing neutron absorption (78 % as compared to 85 %).

Configuration ${}^6\text{LiF}:\text{ZnS}:\text{binder}$	Neutron Absorption (%) (0.42 mm thickness)	Light Transmission (%) Diffuse (@450 nm)
1:2:0.30	83	1.85
1:2:0.45	78	3.67
1:2:0.60	75	4.76
1:2:0.75	74	4.77

Table 1: Neutron capture probability and light transmission for diffuse transmission measurements at 450 nm. The actual detector sensitivity is set by both parameters; therefore, the optimal compound should be selected based on the allowed physical dimensions.

GEANT4 simulations indicate that the grain sizes of both the ${}^6\text{LiF}$ and the ZnS(Ag) influence the amount of light produced by a neutron capture. If the ${}^6\text{LiF}$ grains are small, the alpha and triton have a greater chance of transferring energy to the phosphor. If they are large, it is likely that for a neutron captured in the center of the grain the reaction products will lose energy as they leave the grain and will transfer less to the phosphor. The standard average grain size in the scintillator formulation is 4 μm . If the ZnS(Ag) grains are small, the average distance that the heavy ions must traverse prior to encountering the phosphor is short. Figure 6 synthesizes a GEANT4 simulation of the light yield for a scintillator mixture with a weight ratio of 1:2:0.3 and five ZnS(Ag) grain sizes (1 μm , 2 μm , 4 μm , 8 μm , and 16 μm) [17]. The indications are that for smaller grain sizes the light output per neutron capture event is more uniform.

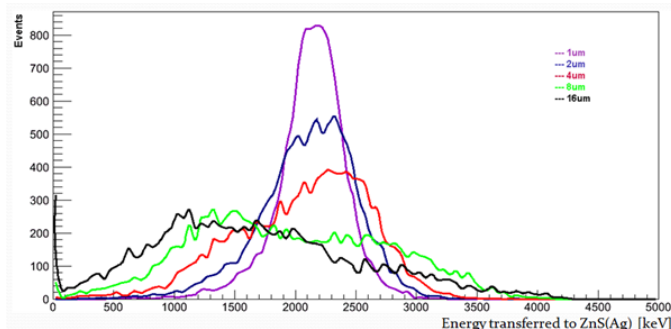


Figure 6: GEANT4 simulation of the light yield for scintillator mixture with a weight ratio of 1:2:0.3 with five different ZnS grain sizes (1 μm , 2 μm , 4 μm , 8 μm , and 16 μm). The narrowing of the distribution indicates that the light output becomes more uniform per capture event as the grain size is reduced.

Light transmission measurements on samples with the same component proportions but different ZnS(Ag) grains sizes indicate that those specimens with smaller grains transmit less light and that adjusting the grain size was not an effective way to improve light production and transmission. We posit that the decrease in transmission could be related to the different index of refraction in the various materials and the increase in the number of grain boundaries that the light must traverse on its way through the medium.

Another factor that begs to be investigated is the homogeneity of the scintillator medium. SEM micrographs (Figure 7) emphasize the possible nonhomogeneous grain distribution of scintillator (1:2:0.3 ${}^6\text{LiF}:\text{ZnS(Ag)}:\text{binder}$) for ZnS(Ag) with an average grain size of 8 μm and with an average grain size of 3 μm . Surprisingly, samples with smaller grains show that those grains cluster together to create larger effective

grains than those observed in materials made with the larger stock grain size. This clustering reduces the ionizing energy transfer of the alpha particle and triton, resulting in lower light yield than in a material with a homogeneous grain distribution.

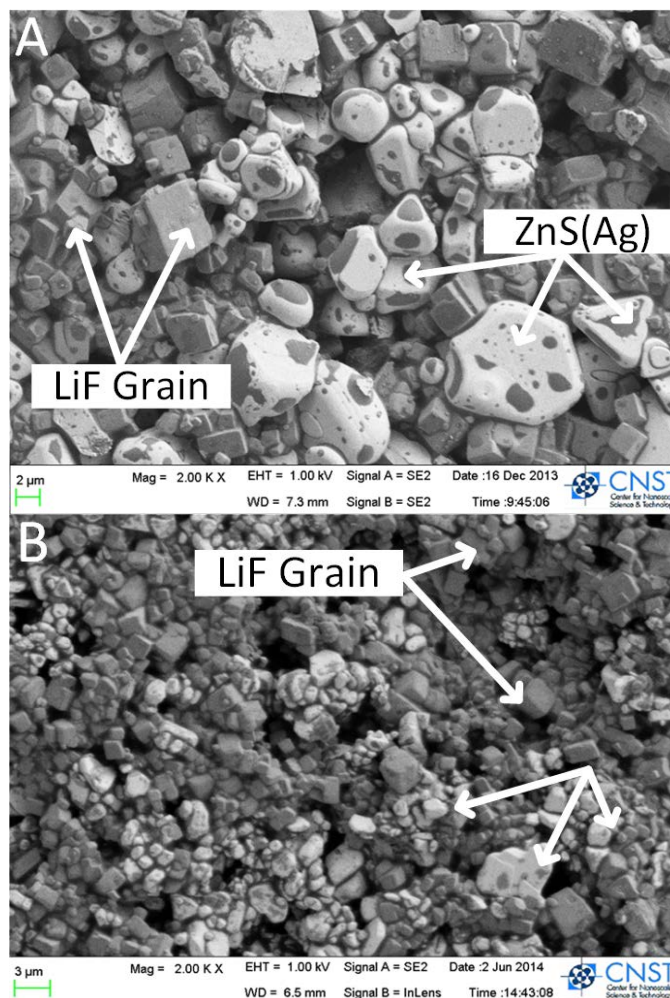


Figure 7: (A) SEM micrograph of 1:2:0.3 scintillator with average ZnS grain size of 8 μm . (B) Micrograph of 1:2:0.3 scintillator with average ZnS grain size of 3 μm . Note in each case that the ZnS grains cluster together to form a larger effective grain size.

Both phenomena (clustering and light attenuation) pointed us in the direction of using the ZnS(Ag) with the standard grain size of 8 μm .

Configuration	ZnS(Ag) Grain Size (μm)	Thickness (mm)	Neutron Absorption (%)	Light Transmission (%)	
				Diffuse @450 nm	Direct @ 450 nm
1:2:0.3	8	0.413	72.3	1.803	0.0132
1:2:0.6	8	0.401	68.6	6.013	0.0488
1:2:0.6	3	0.405	68.8	0.553	0.0225
1:3:0.6	8	0.395	65.0	4.569	0.0356

Table 2: Absorption and light transmission (diffuse and direct) measured at 450 nm for LiF:ZnS(Ag):binder scintillator mixtures

Table 2 synthesizes relative neutron absorption and light transmission data for a number of scintillator mixtures with differing proportions of binder and ZnS(Ag) grain size. Increasing the proportion of binder improves light transmission while slightly decreasing neutron absorption. The 1:2:0.3 mixture, which has the highest ${}^6\text{Li}$ concentration per unit volume, has an absorption of 72.3 %.

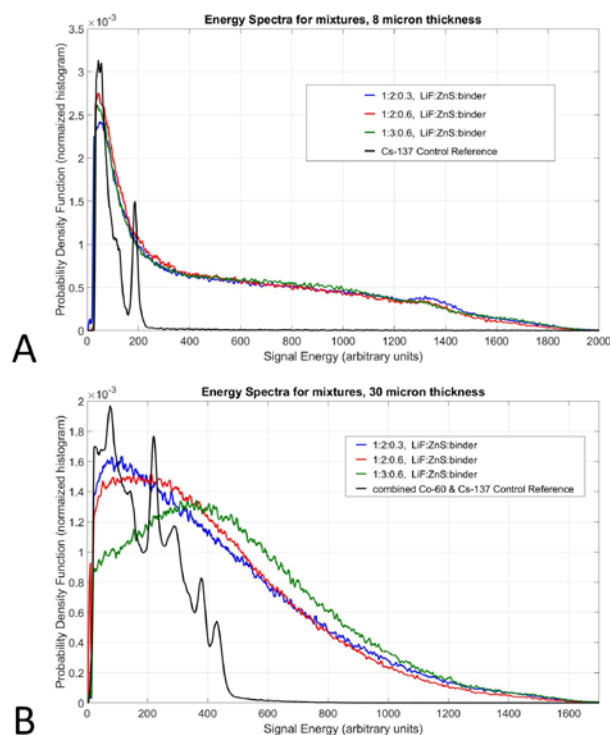


Figure 8: Pulse height spectra measured for A:8 micron- and B:30 micron-thick slabs of scintillator material.

To study the light yield of these different mixtures, we produced thin slabs of material with a thickness of 8 μm (equivalent to a single layer of ZnS(Ag) grains). The geometry of the specimen was intended to have negligible attenuation of the light emitted and to therefore be representative of the light yield affected primarily energy loss of the alpha and the triton prior to ionizing the ZnS(Ag). As the mean free path of the triton in the material is about 40 μm , we also produced a 30 μm slab. This slab thickness has higher probability to be ionized by the alpha and the triton but will also attenuate the produced light. The spectra measured for the mixtures for the 8 μm and 30 μm slabs are shown in Figure 8. The number of events for each mixture was normalized and it became clear that the highest light yield occurs in the mixture with weight ratio 1:3:0.6. The 8 μm thick spectra are mainly dominated by the alpha ionization and therefore the ZnS(Ag) concentration has a major effect on the spectra. In the 30 μm slab the triton is attenuated as well and the light output spectrum measured for the three mixtures has less variation.

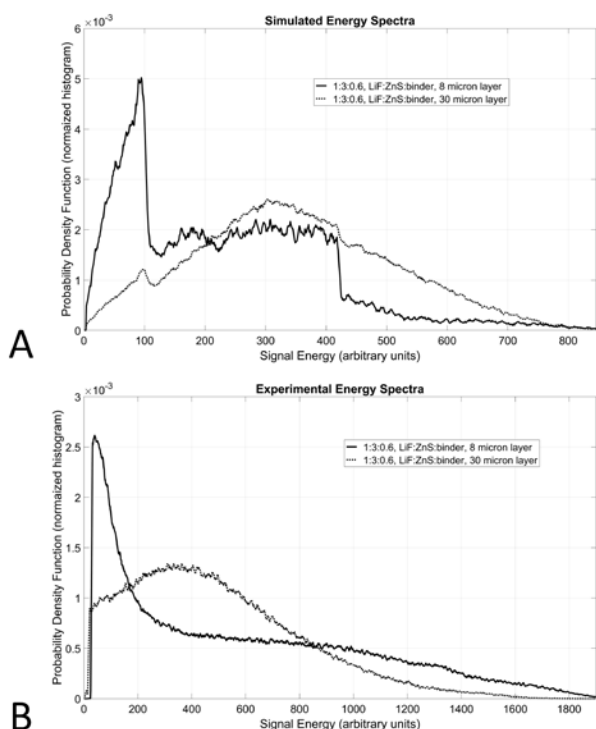


Figure 9: Simulated(A) and experimental(B) pulse height spectra for 8 micron- and 30 micron-thick slabs of scintillator.

The spectra for all three scintillator weight ratios 1:2:0.3, 1:2:0.6, and 1:3:0.6 have similar maximal light yield but the difference in the shape of spectra is correlated with the detection probability. Spectra whose centroids are shifted to higher energies are indications of better neutron discrimination. Even so, the overall sensitivity is influenced by our ability to capture events with small light yield.

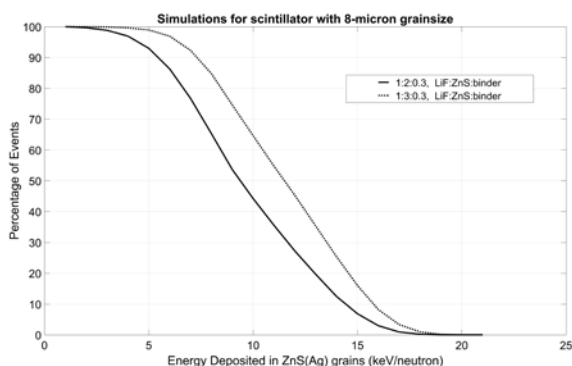


Figure 10: Simulations of energy deposition in scintillator with weight ratios of 1:2:0.3 and 1:3:0.3.

The measured spectrum for the 1:3:0.6 mixture was compared to the light spectrum simulated by GEANT4. As can be seen in Figure 9, there are similarities between the simulated and measured spectra for both the 8 μm slab and the 30 μm slab. The differences between the measured and simulated results might be related to the assessment that the distribution of the ZnS(Ag) grain sizes is similar on both slabs but the 30 μm slab can have some larger effective grain sizes that could affect the measured spectra.

By far the most significant balance to strike is the one between neutron capture and light emission and transport in the weight ratio of ^6LiF to ZnS(Ag). While it would be possible to build a thinner neutron detector using a 1:2:0.6 weight ratio scintillator, simulations indicate that formulations with a higher proportion of ZnS(Ag) (1:3:0.6) would yield more light (Figure 10).

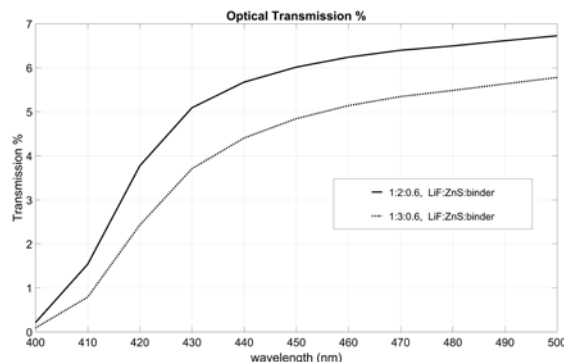


Figure 11: Light transmission measurements for scintillator weight ratios of 1:2:0.6 and 1:3:0.6.

Figure 11 shows wavelength dependent light transmission measurements for 0.42 mm thick samples of 1:2:0.6 and 1:3:0.6 scintillators. Figure 12 shows pulse height distributions measured for a detector using the 1:2:0.6 mixture with a thickness of 1.1 mm and a detector using the 1:3:0.6 mixture with a thickness of 1.35 mm. Both detectors have the same neutron absorption (90 %). The two figures illustrate that the light production for the 1:3:0.6 mixture is higher than for the 1:2:0.6 and that although the light attenuation of the 1:3:0.6 with the thicker detector is higher, this weight ratio is preferred if a thicker detector is permitted (thickness increase of 15 %).

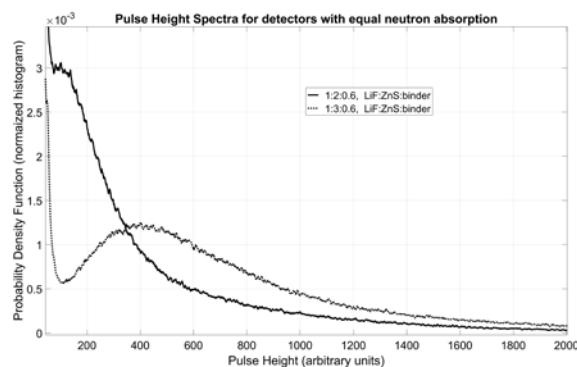


Figure 12: Pulse height distributions measured for scintillators with weight ratios of 1:2:0.6 (solid) and 1:3:0.6 (dotted). Both samples have thicknesses tuned such that the neutron capture probability is 90% for 3.27 meV neutrons.

Our basic assumption was that the mixture consists only of the three components (^6LiF , ZnS(Ag), and binder). However, the neutron capture probability predicted by GEANT4 simulations was higher than our measurements. On investigation, SEM imaging studies revealed the existence of air bubbles in the material. These voids scatter light passing through the medium and contribute to additional losses. Both effects reduce the net detection sensitivity. This prompted us to change the production process by mechanically pressing the scintillator around the WLS fibers to remove voids. After

pressing, volume measurements indicate that the mass density increased by 25 % and approached the estimates used for the simulation. Light transmission curves for pressed and unpressed sheets of scintillator are shown in Figure 13. The neutron absorption before and after the pressing did not change, but the amplitude of the average light signal did increase, improving the net sensitivity of the detector.

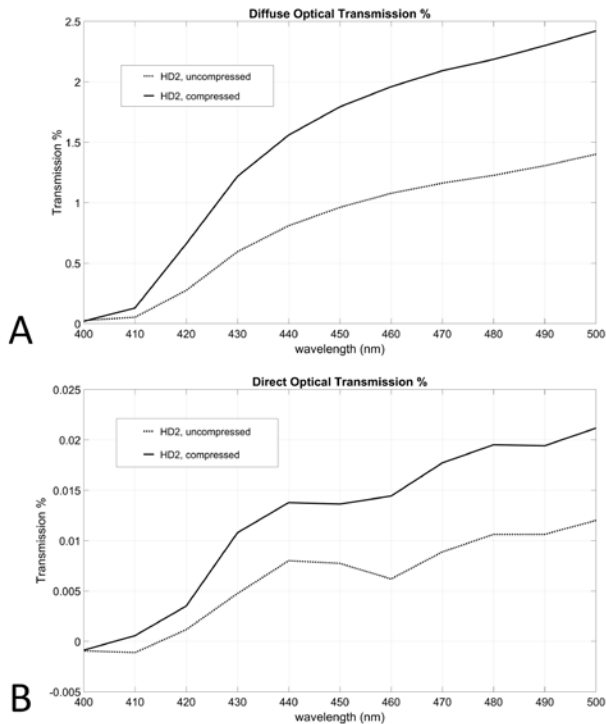


Figure 13: Diffuse (A) and Direct (B) light transmission versus wavelength for compressed mixture (solid) and uncompressed mixture (dotted).

In the interests of manufacturability and keeping the neutron absorption high and thickness minimized, we elected to use slabs of the manufacturer's standard 1:2:0.14 mixture backed on reflector material in the final version of the detector. After pressing, the overall thickness of the detector was 1.04 mm. These detectors have a typical neutron sensitivity of 85% for 3.27 meV (5 \AA) neutrons with gamma rejection ratios on the order of 10^{-7} [2].

In the above studies, we have experienced relative improvements in the light spectra of the different mixtures as a function of the different parameters we have been able to adjust. However, as part of the optimization process we have also tried to determine the absolute light yield compared to the 160,000 light photons per neutron anecdotally cited by other researchers.

The absolute light output of the scintillator was measured [18] with a setup made by Scionix Holland. The apparatus was based on the ET9104 PMT and a voltage divider which enables locating a scintillator sample directly over the photocathode. The output signal was connected to a Multichannel Analyzer. We placed the 30 μm slabs of three different mixture weight ratios 1:2:0.3, 1:2:0.6 and 1:3:0.6 in front of the neutron beam and measured the pulse height spectrum. We then coupled a CsI(Na) scintillation crystal to the PMT without changing the PMT operating voltage or amplification. Because the CsI(Na)

scintillation crystal was a cylinder with thickness of 15 mm, we used a reflector to cover two surfaces, the one facing the PMT and the upper one. This configuration enables the light produced in the crystal either to reach the PMT or to escape from the upper surface, a condition similar to the measurement of the ${}^6\text{LiF:ZnS(Ag)}$ slab with the neutrons. We located ${}^{137}\text{Cs}$ and ${}^{60}\text{Co}$ sources next to the CsI(Na) scintillation crystal and measured the spectra.

The CsI(Na) crystal was selected for this study because it has an emission wavelength of 440 nm, which is similar to the emission wavelength of the ZnS(Ag). The crystal has a light yield of 35,000 light photons per MeV, meaning about 23,000 light photons for the ${}^{137}\text{Cs}$ gamma emission of 662 keV and about 46,000 light photons for the ${}^{60}\text{Co}$ gamma emission of 1,330 keV. The gamma photopeaks of the two isotopes were measured at channels 220 and 440, presenting a linear conversion of about 3 keV per channel or about 105 light photons per channel. If we divide the 160,000 light photons per neutron interaction by the calculated conversion factor, we find that the maximal neutron light yield should be around channel 1,600, corresponding well with our measurement. This result confirms not only the literature data but shows that this is a maximal value.

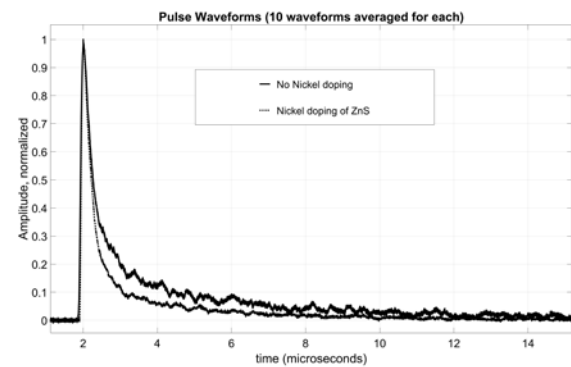


Figure 14: Doping the ZnS phosphor with nickel (dotted curve) shortens the decay time of the neutron capture signal over the undoped phosphor (solid curve).

One of the challenges that the ${}^6\text{LiF:ZnS(Ag)}$ mixture presents is its long signal decay in the case of events with a large light signature (Figure 3). This phenomenon could cause a single event to be counted twice. Previous work demonstrated the correlation between the decay time and the amount of nickel added to the phosphor [19] [20] [21] [22]. We fabricated two detectors with similar geometry and mixture stoichiometry, but used a nickel doped ZnS(Ag) phosphor in one. Neutron capture waveforms for these two detectors are shown in Figure 14. The nickel doping shortens the decay time of the signal, reducing the amplitude in the tail region by half in 8 μs . The advantage of this doping is that it lowers the probability of multiple counting for neutron events. The disadvantage is that there is less amplitude in the tail for neutron/gamma discrimination.

We elected to use this nickel doped scintillator in a layer immediately surrounding the WLS fibers on the principle that capture events occurring nearest the WLS fibers are most likely to exhibit the propensity for event pileup.

IV. DISCUSSION

We have presented the optimization of an ultrathin cold neutron detector using ${}^6\text{LiF}:\text{ZnS}(\text{Ag})$ scintillator as the neutron converter. Because of the opacity of ZnS to its own luminescence we have studied the use of different weight ratios of the neutron converter, phosphor, and binder to find a composition that combines high neutron capture probability with strong light output and good light transport.

It is essential in this ultrathin design to use WLS fibers to conduct the scintillation light away from the neutron sensitive portion of the detector to a photo sensor given that both the light absorption in the WLS fiber and the photodetection efficiency are low ($\approx 5\%$ and 45% respectively). The optimum mixture of components was found to be that which ensured the greatest light production. Additionally, we have demonstrated the importance of pressing out voids in the scintillator mixture to improve light transport. Considerations related to the properties of the photosensor [23] and the discrimination algorithm [16] are reported in other articles.

In efforts to reduce the probability of inadvertently counting the same neutron capture event more than once, we have doped the ZnS phosphor with nickel. This has the effect of reducing the decay time of the trailing edge of the neutron capture waveform.

These considerations have led us to a multilayered arrangement of scintillator with embedded WLS fibers. The innermost ("primer") layer painted around the WLS fibers had a composition of 1:2:0.6 with nickel doped phosphor to reduce the amplitude of the neutron capture decay envelope to reduce the likelihood of multiple counting. The outermost layers were slabs of reflector-backed 1:2:0.14 pressed into the primer layer. Following pressing the average thickness is 1.04 mm.

The expectation is that detectors of this type which both efficiently detect and energy analyze the scattered neutrons, will be incorporated into many new neutron scattering instruments and that the neutron sensitive elements themselves could even be used as standalone detectors for many different applications.

V. DISCLAIMER

Certain trade names and company products are identified to adequately specify the experimental procedure. In no case does such identification imply recommendation or endorsement by the National Institute of Standards and Technology, nor does it imply that the products are necessarily the best for the purpose.

VI. REFERENCES

- [1] C. F. Majkrzak, "CANDOR Spectrometer," [Online]. Available: <http://www.ncnr.nist.gov/instruments/CANDOR>.
- [2] A. N. Osovizky, K. M. Pritchard, Y. Yehuda-Zada, J. B. Ziegler, E. Binkley, P. Tsai, A. Thompson, N. Hadad, M. Jackson, C. Hurlbut, G. M. Baltic, C. F. Majkrzak and N. C. Maliszewskij, "Design of an Ultrathin Cold Neutron Detector," *Nucl. Inst. and Meth. A*, in press.
- [3] Eljen Technologies, USA, "Thermal Neutron Detector EJ-426," [Online]. Available: <http://www.eljentechnology.com/products/neutron-detectors/ej-426>.
- [4] C. W. E. Van Eijk, A. Bessiere and P. Dorenbos, "Inorganic Thermal Neutron Scintillators," *Nucl. Inst. and Meth. A*, vol. 529, pp. 260-267, 2004.
- [5] C. W. E. Van Eijk, "Neutron PSDs for the Next Generation of Spallation Neutron Sources," *Nucl. Inst. and Meth. A*, vol. 477, pp. 383-390, 2002.
- [6] C. W. E. Van Eijk, "Inorganic Scintillator Development," *Nucl. Inst. and Meth. A*, vol. 460, pp. 1-14, 2001.
- [7] V. S. Litvin, A. D. Beyaev and S. M. Ignatov, " $\text{ZnS}(\text{Ag})/6\text{LiF}$ and $\text{LiI}(\text{Eu})$ Scintillators and Silicon Photomultipliers for Thermal Neutron Detectors with High Space and Time Resolution," *Bulletin of the Russian Academy of Sciences: Physics*, vol. 73, pp. 219-221, 2009.
- [8] Bicon USA, " $\text{ZnS}(\text{Ag})$ Phosphor," [Online]. Available: http://www.hep.ph.ic.ac.uk/fets/pepperpot/docs+papers/zns_602.pdf.
- [9] V. S. Marin, R. A. Saykov and D. N. Trunov, "A New Type of Thermal Neutron Detector Based on $\text{ZnS}(\text{Ag})/\text{LiF}$ Scintillator and Avalanche Photodiodes," *Technical Physics Letters*, vol. 41, no. 9, pp. 912-914, 2015.
- [10] W. Chong, B. Tang, Z. Sun, Q. Zhang, W. Luo and T. Wang, "The Monte Carlo Simulation on a Scintillator Neutron Detector," *Science China Physics*, vol. 56, no. 10, pp. 1892-1896, 2013.
- [11] G. Blasse and B. C. Grabmaier, *Luminescent Materials*, Berlin: Springer, 1994.
- [12] G. F. Knoll, *Radiation Detection and Measurement*, 4 ed., New York: John Wiley and Sons, 1999, p. 245.
- [13] M. David, A. Gomes, A. Maio, A. Henriques, Y. Protopopov, D. Jankowski and R. Stanek, "Comparative Measurements of WLS Fibers," 1994. [Online]. Available: <http://cds.cern.ch/record/683488/files/tilecal-94-034.pdf>.
- [14] S. Agostinelli, J. Allison and K. Amako, "Geant4 - a Simulation Toolkit," *Nucl. Inst. and Meth. A*, vol. 506, pp. 250-303, 2003.
- [15] Carl Zeiss Microscopy GmbH, "NIST Scanning Electron Microscope," [Online]. Available:

<https://www.nist.gov/laboratories/tools-instruments/nanofab-tool-zeiss-ultra-60-field-emission-scann>.

- [16] K. M. Pritchard, A. N. Osovizky, J. B. Ziegler, E. Binkley, P. Tsai, N. Hadad, M. Jackson, C. Hurlbut, G. M. Baltic, C. F. Majkrzak and N. C. Maliszewskyj, "Computational Techniques for Optimizing Performance of a LiF:ZnS(Ag) Neutron Detector using Recorded Waveforms," *In Preparation*.
- [17] Y. Yehuda-Zada, K. Pritchard, J. B. Ziegler, C. Cooksey, K. Siebein, M. Jackson, C. Hurlbut, Y. Kadmon, Y. Cohen, R. M. Ibberson, C. F. Majkrzak, N. C. Maliszewskyj, I. Orion and A. Osovizky, "Optimization of 6LiF:ZnS(Ag) Scintillator Light Yield Using GEANT4," *Nucl. Instr. and Meth A*, in press.
- [18] M. I. Arsaev and A. V. Kladov, "Comparative Characteristics of PC-450 and PC-4 Phosphors Based on ZnS(Ag) Phosphor," *Instruments and Experimental Techniques*, vol. 52, no. 2, pp. 183-186, 2009.
- [19] M. Katagiri, K. Sakasai and M. Masubayashi, "Neutron/Gamma Ray Discrimination Characteristics of Novel Neutron Scintillators," *Nucl. Inst. and Meth. A*, vol. 529, pp. 317-320, 2004.
- [20] K. T. Rasoul, N. K. Abbas and Z. J. Sharan, "Structural and Optical Characterization of Cu and Ni Doped ZnS Nanoparticles," *Int. Journal of Electrochemical Science*, vol. 8, pp. 5594-5604, 2013.
- [21] V. Ramaswamy, K. Praba and G. Murugadoss, "Synthesis and Study of Optical Properties of Transition Metal Doped ZnS Nanoparticles," *Molecular and Biomolecular Spectroscopy*, vol. 96, pp. 963-971, 2012.
- [22] H. Iikura, N. Tsutsui and T. Nakamura, "Evaluation of new LiF-Scintillator and Optional Brightness Enhancement Films for Neutron Imaging," *Nucl. Inst. and Meth. A*, vol. 651, pp. 100-104, 2011.
- [23] A. N. Osovizky, K. M. Pritchard, Y. Yehuda-Zada, J. B. Ziegler, P. Tsai, M. Ghelman, A. K. Thompson, R. M. Ibberson, G. M. Baltic, C. F. Majkrzak and N. C. Maliszewskyj, "Selection of Silicon Photomultipliers for a 6LiF:ZnS(Ag) Scintillator Based Neutron Detector," *In Preparation*.
- [24] Y. Yehuda-Zada, I. Orion, L. Dongwon, O. Hen, A. Beck, K. Kadmon, Y. Cohen, J. Ziegler, N. C. Maliszewskyj and A. Osovizky, "Monte Carlo Simulation for Optimizing 6LiF:ZnS(Ag) Based Neutron Detector Configurations," in *27th Conference of the Nuclear Societies in Israel*, 2014.
- [25] D. S. McGregor, M. D. Hammin and Y. H. Yang, "Design Considerations for Thin Film Coated Semiconductor Thermal Neutron Detectors," *Nucl. Inst. and Meth. A*, vol. 500, pp. 272-308, 2003.